Enhanced Ni-Al-Based Catalysts and Influence of Aromatic Hydrocarbon for Autothermal Reforming of Diesel Surrogate Fuel

Dong Geon Ju [1,2,†], Seong Bin Jo [3,†], Dong Su Ha [4], Tae Young Kim [1], Suk Yong Jung [5], Ho Jin Chae [3] , Soo Chool Lee [3,*] and Jae Chang Kim [1,*]

[1]   Department of Chemical Engineering, Kyungpook National University, Daegu 41566, Korea
[2]   Korea Evaluation Institute of Industrial Technology (KEIT), Daegu 41069, Korea
[3]   Research Institute of Advanced Energy Technology, Kyungpook National University, Daegu 41566, Korea
[4]   Korea Institute of Energy Research, Daejeon 34129, Korea
[5]   Wonik Materials Co., Cheongju 28125, Korea
[*]   Correspondence: soochool@knu.ac.kr (S.C.L.); kjchang@knu.ac.kr (J.C.K.);
      Tel.: +82-53-950-5622 (J.C.K. & S.C.L.)
[†]   Dong Geon Ju and Seong Bin Jo contributed equally to this work.

Abstract: Aromatic hydrocarbons along with sulfur compounds in diesel fuel pose a significant threat to catalytic performances, due mainly to carbon deposition on the catalytic surface. In order to investigate the influence of an aromatic hydrocarbon on the autothermal reforming of diesel fuel, 1-methylnaphthalene ($C_{11}H_{10}$) was selected as an aromatic hydrocarbon. Two types of diesel surrogate fuel, i.e., DH (dodecane ($C_{12}H_{26}$) and hexadecane ($C_{16}H_{34}$) mixture) as well as DHM (DH fuel and $C_{11}H_{10}$ mixture) fuel, were prepared. A Rh-Al-based catalyst (R5A-I) was prepared using a conventional impregnation method. Various Ni-Al-based catalysts with Fe and Rh promoters were prepared via a polymer modified incipient method to improve the carbon coking resistance. These catalysts were tested under conditions of S/C = 1.17, O_2/C = 0.24, 750 °C, and GHSV = 12,000 h^{-1} at DH or DHM fuel. R5A-I exhibited excellent catalytic performance in both DH and DHM fuels. However, carbon coking and sulfur poisoning resistance were observed in our previous study for the Ni-Al-based catalyst with the Fe promoter, which became deactivated with increasing reaction time at the DHM fuel. In the case of the Rh promoter addition to the Ni-Al-based catalysts, the catalytic performances decreased relatively slowly with increasing (from 1 wt.% (R1N50A) to 2 wt.% (R2N50A)) content of Rh_2O_3 at DHM fuel. The catalysts were analyzed via scanning electron microscopy combined with energy dispersive X-ray, X-ray diffraction, and X-ray photoelectron spectroscopy. Gas chromatography-mass spectrometry detected various types of hydrocarbons, e.g., ethylene (C_2H_4), with catalyst deactivation. The results revealed that, among the produced hydrocarbons, C_2H_4 played a major role in accelerating carbon deposition that blocks the reforming reaction. Therefore, Rh metal deserves consideration as a carbon coking inhibitor that prevents the negative effects of the C_2H_4 for autothermal reforming of diesel fuel in the presence of aromatic hydrocarbons.

Keywords: autothermal reforming; dodecane; hexadecane; 1-methylnaphthalene; nickel; rhodium; diesel; aromatic hydrocarbon

1. Introduction

Compared with other energy sources, hydrogen energy represents a cleaner and more sustainable energy, and has become one of the clean fuel options for reducing motor vehicle emissions. Hydrogen can be produced from a mixture of clean coal, fossil fuels, and nuclear power [1]. A hydrogen energy

system is a complex system that includes production, utilization, and storage parts, and hydrogen utilization is difficult, due to the lack of hydrogen-supply infrastructure. In particular, hydrogen storage in safe, inexpensive, and lightweight storage vessels has been accomplished [2,3]. Furthermore, auxiliary power unit (APU) systems have been considered as on-board fuel processors. Hydrocarbon fuels, such as gasoline and diesel fuel, are used to operate the engines of most vehicles. Hydrogen, which is attainable through a catalytic reforming process performed on hydrocarbon fuels, can be used to generate electrical energy for fuel cells [4–6]. Notably, solid oxide fuel cell (SOFC)-based APU systems that use diesel fuel are unique alternatives because this fuel takes advantage of the high hydrogen density and existing fuel infrastructure [7–9]. Various reforming methods, including steam reforming (SR), partial oxidation (POX), and autothermal reforming (ATR), may be used to generate hydrogen-rich gases for APU systems. A water gas shift reaction (WGSR) may occur in the presence of CO and excessive steam. The corresponding reforming reactions are given as follows:

(1)   SR: $C_nH_m + nH_2O \rightarrow (m/2+n)H_2 + nCO$
(2)   POX: $C_nH_m + (n/2)O_2 \rightarrow (m/2)H_2 + nCO$
(3)   ATR: $C_nH_m + (n/2)H_2O + (n/4)O_2 \rightarrow (m+n)/2H_2 + nCO$
(4)   WGSR: $CO + H_2O \leftrightarrow H_2 + CO_2$

ATR combines endothermic SR with exothermic POX. In other words, hydrocarbon fuels react with air and steam, which generates hydrogen-rich gas. Compared with the conventional reforming methods, ATR as a potential reforming method exhibits higher energy efficiency and thermal stability [10–17]. The production technologies of green diesel have studied for combustion engines with remarkable properties and significantly lower emissions [18]. The complexity of a typical commercial diesel fuel composition prevents exact modeling of such compositions. Due to sulfur poisoning and carbon deposition, low aromatic and sulfur compounds in diesel fuels lead to significant deterioration of the catalytic performance [19–21]. Many catalysts have been prepared and tested for reforming hydrocarbon fuel. Methane, biogas, and glycerol were employed as feedstock for the production of syngas (CO + H_2) as well as gasoline and diesel fuel [22–25]. Additionally, the role of the oxide support in the catalytic performance of ATR performed on a gasoline surrogate fuel was determined by testing Rh catalysts with various supports (Gd-CeO_2, Y-ZrO_2, γ-Al_2O_3, La-Al_2O_3, and $CaAl_{12}O_{19}$) [26]. Ni-catalysts supported on modified alumina (-La, -Ba, and -Ce) were studied with the aim to improve the catalytic performance associated with steam reforming of diesel fuel [27]. Pt/CeO_2-Al_2O_3 was investigated for numerical simulation of diesel reforming [28]. Rh-Ni-based catalysts showed high activity and stability for methane reforming by the addition of Rh [29,30]. Jet fuel in the absence and presence of sulfur was conducted by Rh and Rh–Ni loaded on CeO_2-modified Al_2O_3 support for steam reforming [31]. Furthermore, novel-metal-based (RhPt/ZrO_2, Al_2O_3, CeO_2-ZrO_2, SiO_2, and TiO_2, Rh-Ni/Al_2O_3) catalysts were evaluated for reforming diesel fuel in the presence of sulfur compounds [32–36]. Rh-based catalysts were prepared via microemulsion and a zone-coating preparation method for diesel reforming [37,38] and also sorption-hydrolytic deposition conducted for highly dispersed Rh-, Pt-, and Ru/$Ce_{0.75}Zr_{0.25}O_2$–δ catalysts [39]. Rh/$Ce_{0.75}Zr_{0.25}O_{2\text{-}\delta}$-$\eta$-$Al_2O_3$/FeCrAl were tested in pilot scale reactors with autothermal reforming of n-hexadecane. The produced syngas can be supplied as a fuel for power generation units based on SOFC [40]. In our previous studies, a polymer modified incipient method (PM) was introduced as a timesaving and promising alternative preparation method to conventional preparation methods, such as impregnation or co-precipitation methods [41]. Moreover, sulfur-resistant Ni-Al-based catalysts with added Fe promoters were prepared by means of the PM method for autothermal reforming of dodecane [42]. The role of these catalysts in diesel surrogate fuel containing aromatic hydrocarbons has, however, remained unexplored. Therefore, in this study, Ni-Al-based catalysts were tested in the presence of aromatic hydrocarbon such as 1-methylnaphthalene ($C_{11}H_{10}$) and, ultimately, attempt to enhance catalytic performances. The ethylene (C_2H_4) was considered a major contributor to catalyst deactivation that results in rapid coke formation during the reforming process [43,44]. The produced hydrocarbons (e.g., C_2H_4) were detected via

GC-MS to identify the hydrocarbon that plays the major role in this deactivation in the presence of aromatic hydrocarbon. Furthermore, the catalysts were characterized by means of field emission scanning electron microscopy (FE-SEM) in conjunction with energy dispersive X-ray (EDX), X-ray diffraction (XRD), and X-ray photoelectron spectroscopy (XPS).

2. Results and Discussion

2.1. Catalytic Performances in the Absence and Presence of Aromatic Hydrocarbon

The experiments were performed at S/C = 1.17, O_2/C = 0.24, 750 °C, and GHSV = 12,000 h^{-1}, for comparison with the catalytic performances realized in the presence of aromatic hydrocarbons such as 1-methylnaphthalene ($C_{11}H_{10}$). Figure 1 shows the conversions obtained for the blank test, R5A-I, N10A, and F10N10A at DH (dodecane ($C_{12}H_{26}$) and hexadecane ($C_{16}H_{34}$) mixture) and DHM (DH fuel and $C_{11}H_{10}$ mixture) fuels. A conversion of ~33% was obtained for the blank test, with/without $C_{11}H_{10}$ in the diesel surrogate fuel. As shown in Figure 1a, conversions of ~80% were obtained for 5-hour periods of each catalyst at the DH fuel. However, the catalytic performances varied with the addition of $C_{11}H_{10}$ to the diesel surrogate fuel (see Figure 1b). The catalytic performances of N10A and F10N10A deteriorated significantly within 1 hour and, thereafter, the conversions remained the same as that of the blank test, which suggests that the catalysts were completely deactivated. The addition of Fe as a promoter to Ni-Al-based catalysts enhances carbon coking and the sulfur poisoning resistance, as reported in our previous study [42]. However, this addition had a negative effect in the presence of the aromatic hydrocarbon. Although the conversion of R5A-I at DHM fuel was 10% lower than that at the DH fuel, the catalytic performance of R5A-I was maintained for 5 hours. This indicated that R5A-I including Rh metal acted as an excellent catalyst at the DHM fuel.
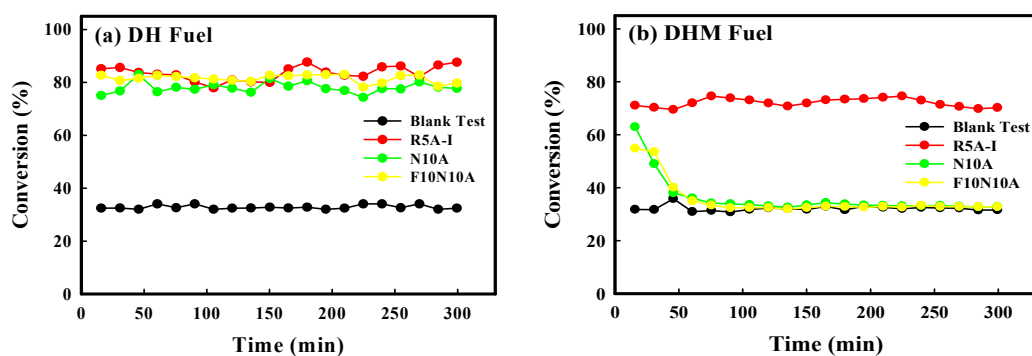

Figure 1. Conversions corresponding to the blank test, R5A-I, N10A, and F10N10A at: (**a**) DH and (**b**) DHM fuel.

The selectivity of product gas (%) of the blank test, R5A-I, N10A, and F10N10A at DH and DHM fuel is shown in Figure 2. For the blank test and R5A-I, the percentage of H_2, CO, CH_4, and CO_2 produced in the absence and presence of $C_{11}H_{10}$ was almost the same. Additionally, at the DH fuel, selective percentages of H_2, CO, CH_4, and CO_2 produced by R5A-I was similar to those generated by N10A and F10N10A. Approximately 59%, 23%, 1%, and 17% of H_2, CO, CH_4, and CO_2 selectivity, respectively, were initially generated by deactivated catalysts such as N10A and F10N10A. The subsequent selectivity were nearly the same as those obtained for the blank test. In other words, selectivity of H_2 and CO_2 produced by N10A and F10N10A decreased with increasing time, while that of CO and CH_4 increased until these catalysts were completely deactivated. Therefore, compared with the presence of $C_{11}H_{10}$, reaction conditions, such as S/C, O_2/C, and temperature, played a greater role in selectivity of product gas (%), which is consistent with the findings of our previous study [45].
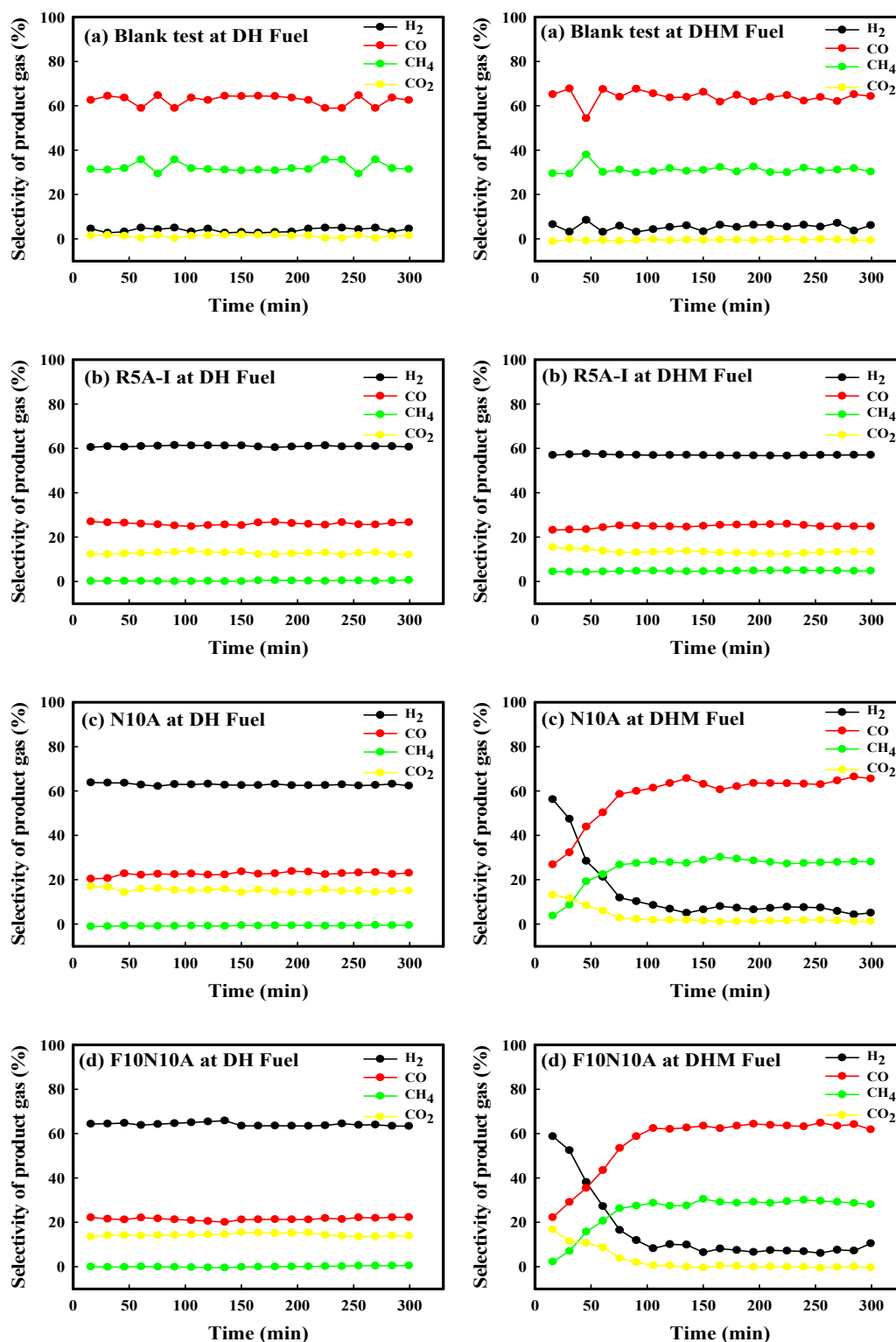
Figure 2. The selectivity of product gas (%) of the (**a**) blank test, (**b**) R5A-I, (**c**) N10A, and (**d**) F10N10A at DH and DHM fuel.

The hydrocarbons produced after reforming were separately analyzed via GC-MS (see Table 1 for the blank test, R5A-I, N10A, and F10N10A data corresponding to 30-minute and 60-minute reactions at the DHM fuel). Small amounts of benzene (C_6H_6) were produced in the case of R5A-I, but various types of hydrocarbons, which resulted in catalyst deactivation, were detected in N10A and F10N10A. High fractions of ethylene (C_2H_4) formed in N10A and F10N10A after 60 minutes of reaction. The previously

mentioned results suggested that the hydrocarbons produced after reforming had an adverse effect on the catalytic performance.

Table 1. Data obtained from the GC-MS of the blank test, R5A-I, N10A, and F10N10A after 30-minute and 60-minute reactions at the DHM fuel.

	Blank Test		R5A-I		N10A		F10N10A	
Reaction Time (min)	**30**	**60**	**30**	**60**	**30**	**60**	**30**	**60**
Carbon dioxide (CO_2)	8.2	8.2	98.3	98.2	39.5	21.2	55.7	25.8
Ethane (C_2H_6)	2.3	2.3	-	-	3.2	2.8	2.9	2.7
Ethylene (C_2H_4)	32.2	32.2	-	-	28.6	30.9	20.7	29.9
Propylene (C_3H_6)	16.4	16.4	-	-	13.1	15.9	7.8	14.7
1,3-Butadiene (C_4H_6)	9.4	9.4	-	-	4.9	8.1	3.0	7.7
1,3-Cyclopentadiene (C_5H_6)	4.5	4.5	-	-	0.9	2.9	0.4	2.6
Benzene (C_6H_6)	16.2	16.2	0.2	0.3	9.7	11.1	7.9	11.7
Toluene (C_7H_8)	4.2	4.2	-	-	-	2.4	1.1	2.1

2.2. Catalyst Analysis before and after Reaction in the Absence and Presence of Aromatic Hydrocarbon

Catalyst deactivation by hydrocarbons production was verified via SEM-EDX, XRD, and XPS analysis. The morphology and amounts of carbon on the catalytic surface were determined by SEM-EDX analysis. High-magnification (10,000x) SEM images reveal the wire shape of carbon deposited on the surface of N10A and F10N10A after a 5-hour reaction at DH and DHM fuel (see Figure 3). Moreover, the amount of carbon coking at DH fuel was expected to be lower than that at the DHM fuel because the previously mentioned wire shape occurred more frequently at DHM fuel. The amounts of carbon on the catalytic surface of R5A-I, N10A, and F10N10A after 5-hour reactions at DH and DHM fuel are listed in Table 2. In the case of R5A-I, ~21 wt.% of carbon occurred on the surface irrespective of the diesel surrogate fuel considered. At the DHM fuel, 47.21 wt.% and 45.08 wt.% of carbon were deposited on the catalytic surface of N10A and F10N10A, respectively, and these amounts were more than twice those occurring at DH fuel. In our previous study, Ni-Al-based catalyst and Fe-Ni-Al-based catalyst at D fuel ($C_{12}H_{26}$) in the presence of DBT were 33.4 wt.% and 8.58 wt.%, respectively [42]. In particular, the amount of carbon increased more in the case of Fe-Ni-Al-based catalyst at DHM fuel, compared to those at D fuel in the presence of DBT and DH fuel. Thus, it was concluded that the addition of Fe to Ni-Al-based catalyst had no effect to prevent carbon deposition on the catalytic surface. Moreover, SEM-EDX analysis revealed that hydrocarbon production promotes carbon deposition on the catalytic surface.
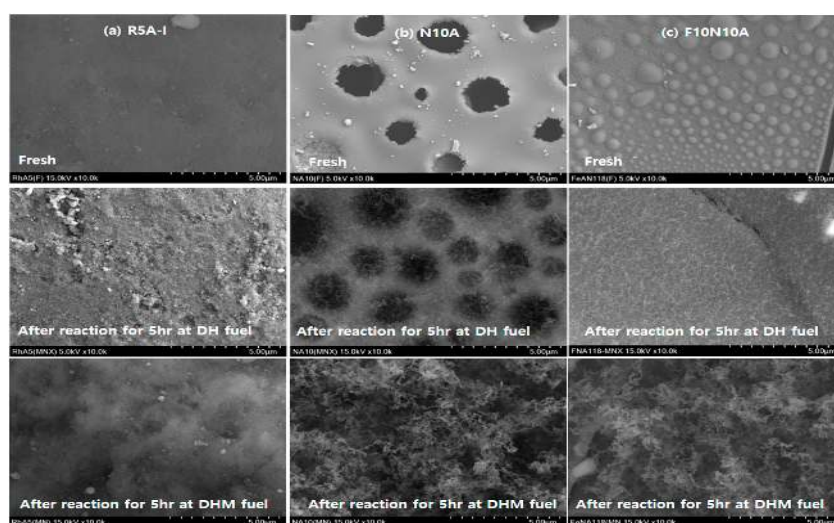

Figure 3. Scanning electron micrographs of (**a**) R5A-I, (**b**) N10A, and (**c**) F10N10A.

Table 2. Amounts of carbon on the catalytic surface of R5A-I, N10A, and F10N10A after 5-hour reactions at DH and DHM fuel.

	R5A-I		N10A		F10N10A	
Fuel	DH	DHM	DH	DHM	DH	DHM
Carbon (wt.%)	21.59	20.89	19.96	47.21	20.78	45.08

The crystal structure of R5A-I, N10A, and F10N10A were characterized via X-ray diffraction (XRD) analysis (see Figure 4). Rh_2O_3, NiO, and Fe_2O_3 were undetected in the fresh state. The incorporation of Ni^{2+} ions into $-Al_2O_3$ ($NiAl_2O_4$) resulted in the lattice expansion of $-Al_2O_3$ and, hence, the diffraction peak of $NiAl_2O_4$ is shifted to a lower diffraction angle, i.e., 66.84°, compared with that of $-Al_2O_3$. The $NiAl_2O_4$ phase is inactive in the reforming reaction of hydrocarbons [45–47]. As shown in Figure 4b,c, the Ni and FeNi phase were observed after the H_2 pre-reduction treatment and 5-hour reaction at DH fuel. However, these phases were absent from the XRD pattern associated with the 5-hour reaction at DHM fuel. The XRD pattern of each catalyst was almost identical to those of the fresh state, which suggests that detection of active metals (e.g., Ni or FeNi) was difficult, due to carbon deposition on the catalytic surface.
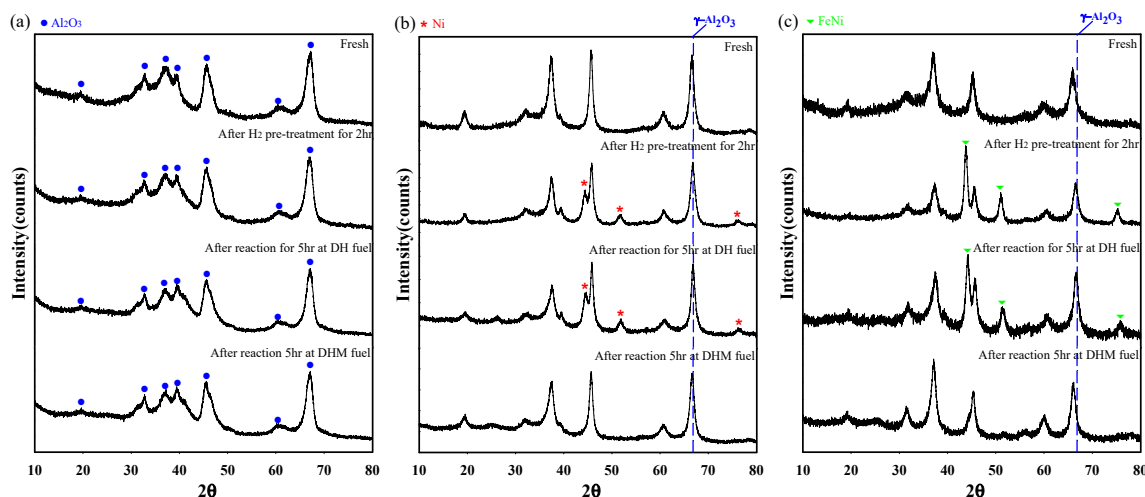
Figure 4. Results of XRD analysis performed on (**a**) R5A-I, (**b**) N10A, and (**c**) F10N10.

The phases comprising R5A-I, N10A, and F10N10A were investigated further via XPS analysis (see Figure 5). Rh_2O_3, NiO, and Fe_2O_3 phases, which were undected by XRD, were observed in the fresh state. The XPS peaks corresponding to Rh3d5/2, Rh_2O_3, and Rh3d3/2 occurred at binding energies of 307.6 eV, 308.3 eV, and 312 eV (see Figure 5a), respectively [48]. The peaks of Rh3d5/2 and Rh3d3/2 appeared after the H_2 pre-reduction treatment and the 5-hour reaction at DH and DHM fuel. The Rh3d5/2 and Rh3d3/2 peaks appearing after this reaction were relatively sharper than those observed after the H_2 pre-reduction treatment. The peaks of Ni, NiO, and $NiAl_2O_4$ are associated with binding energies of 853 eV, 854 eV, and 856 eV, respectively [49], as shown in Figure 5b. However, the 5-hour reaction at DH and DHM fuels yielded indistinguishable Ni peaks. The peaks of FeNi and Fe_2O_3 occurred at binding energies of 710 eV and 711 eV (see Figure 5c), respectively [50]. The FeNi peak after the 5-hour reaction at DHM fuel was slightly smaller than that associated with the 5-hour reaction at DH fuel. The results indicated that the changes in the Ni and FeNi peaks result from carbon deposition on the catalytic surface during the reaction. Therefore, the produced hydrocarons such as C_2H_4 accelerated carbon deposition and inhibited the reforming reaction required for autothermal reforming of the diesel surrogate fuel.
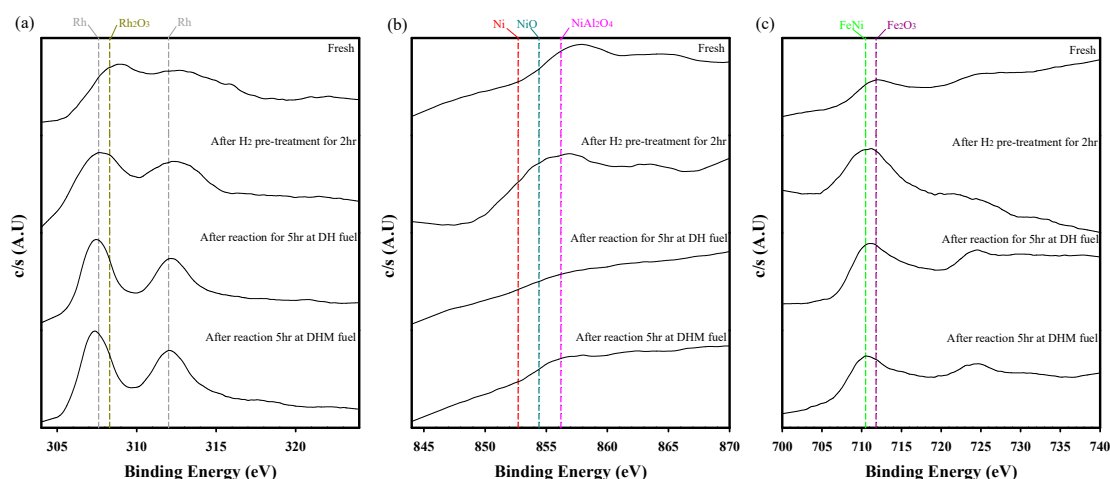
Figure 5. Results of XPS analysis performed on (**a**) R5A-I, (**b**) N10A, and (**c**) F10N10A.

2.3. Catalytic Performances of Ni-Al-Based Catalysts with Fe and Rh Promoters in the Presence of Aromatic Hydrocarbon

The resistance properties of aromatic hydrocarbon were investigated under the previously mentioned conditions. The catalytic performance of Ni-Al-based catalysts improved with increasing content of Ni metal (Supplementary Materials Figure S1). Research regarding the content of Ni metal for autothermal reforming of a diesel surrogate fuel will be presented in another study. Ni-Al-based catalysts with a NiO content of 50 wt.% were prepared and various amounts of Fe and Rh promoters were added to these catalysts to improve and prolong the catalytic performances of DHM fuel. The Ni-Al-based catalysts with different amounts (Fe_2O_3 10 wt.%, 20 wt.%, and 30 wt.%) of Fe promoter were tested using DHM fuel. The Fe promoter improves carbon coking and the sulfur poisoning resistance for autothermal reforming of dodecane [42] and was, hence, expected to prevent carbon deposition in the presence of aromatic hydrocarbons. Figure 6a reveals initial conversions of 72%, 68%, 68%, and 55% for the N50A, F10N50A, F20N50A, and F30N50A, respectively, using DHM fuel. Contrary to expectations, these catalysts were deactivated with increasing reaction time. A conversion of ~33% was obtained for the blank test in Figure 1. This conversion was a similar value with those for the N50A, F10N50A, F20N50A, and F30N50A at higher times. This conversion was obtained from DHM fuel thermally decomposed to CO, CO_2, and CH_4 after catalyst deactivation. Furthermore, catalytic performances of DHM fuel deteriorated with the increasing amount of Fe promoter, i.e., this promoter yielded no improvement in the catalytic performance in the presence of aromatic hydrocarbons, such as $C_{11}H_{10}$. Small amounts (Rh_2O_3 1 wt.% and 2 wt.%) of Rh promoter as alternatives to the Fe promoter were added to the Ni-Al-based catalysts to resolve the problem of catalyst deactivation. Figure 6b reveals an initial conversion of ~70% for the R5A-I, N50A, R1N50A, and R2N50A using DHM fuel. The conversion of R5A-I was maintained for 5 hours, but the catalytic performances of N50A, R1N50A, and R2N50A deteriorated with increasing reaction time. R1N50A and R2N50A were more slowly deactivated than N50A. The deactivation rate of R2N50A was moderately reduced by increasing the content of Rh promoter. The addition of Rh to Ni-Al-based catalysts improved the dispersion of Ni and retarded the sintering of Ni by the strong interaction between Rh and Ni [29,30,33]. Although metallic Rh is a costly metal, the Rh promoter deserves consideration as a promoter for Ni-Al-based catalysts. For improved catalytic performance, further studies are required to identify a suitable promoter that yields autothermal reforming of diesel fuel.
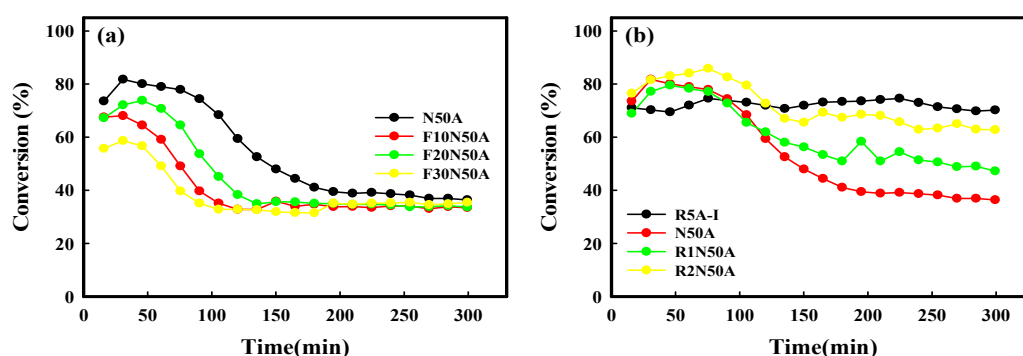
Figure 6. Conversions of the (**a**) N50A, F10N50A, F20N50A, and F30N50A and (**b**) R5A-I, N50A, R1N50A, and R2N50A of DHM fuel.

The basis for differences in the catalytic performance was investigated via GC-MS analysis of hydrocarbons such as C_2H_4. Table 3 shows the data corresponding to R5A-I, N50A, R1N50A, and R2N50A after the reaction for 30-minute and 300-minute using DHM fuel. The amount of hydrocarbons increased, in general, with increasing reaction time, whereas the amount of CO_2 decreased. At fractions of 23.8%, 18.2%, and 16.5%, C_2H_4 accounted for the highest proportion of produced hydrocarbons in the case of N50A, R1N50A, and R2N50A, respectively, which reacted for 300 minutes. C_6H_6 accounted for the second-highest fraction of produced hydrocarbons. Nevertheless, C_6H_6 had a negligible effect on catalyst deactivation, since R5A-I exhibited excellent catalytic performance, despite the high fraction of this hydrocarbon. As previously mentioned, we assumed that the produced hydrocarbons were associated with carbon deposition on the catalytic surface. The results indicated that, compared with the other hydrocarbons, the produced C_2H_4 plays a crucial role in catalyst deactivation, which is consistent with the results of previous studies [43,44]. More importantly, Rh metal seemed to play an important role in reducing C_2H_4 production, which accelerates carbon deposition.

Table 3. Data obtained from GC-MS of R5A-I, N50A, R1N50A, and R2N50A after 30-minute and 300-minute reactions of DHM fuel.

	R5A-I		N50A		R1N50A		R2N50A	
Reaction Time (min)	**30**	**300**	**30**	**300**	**30**	**300**	**30**	**300**
Carbon dioxide (CO_2)	98.3	75.5	94.1	23.8	98.7	38.7	98.7	45.6
Ethane (C_2H_6)	-	0.5	-	2.8	-	2.7	-	2.4
Ethylene (C_2H_4)	-	0.3	-	23.8	-	18.2	-	16.5
Propylene (C_3H_6)	-	-	-	12.2	-	8.8	-	7.9
1,3-Butadiene (C_4H_6)	-	-	-	5.9	-	4.3	-	4.1
1,3-Cyclopentadiene (C_5H_6)	-	-	-	3.5	-	2.7	-	2.7
Benzene (C_6H_6)	0.2	23.7	-	17.9	-	16.6	-	14.1
Toluene (C_7H_8)	-	-	-	4.8	-	4.1	-	3.2

2.4. Analysis of Rh-Ni-Al Catalyst Before and After Reaction in the Presence of Aromatic Hydrocarbon

The morphology and amounts of carbon on the catalytic surface were observed via SEM-EDX analysis. High-magnification (10,000x) SEM images are shown in Figure 7. Wire-shaped carbon occurred in N50A, but classification of the carbon morphology occurring in R5A-I, R1N50A, and R2N50A was difficult. Table 4 lists the amount of carbon formed on each catalytic surface after 5-hour reactions as DHM fuel. As shown, 20.89 wt.%, 40.59 wt.%, 22.05 wt.%, and 21.21 wt.% of carbon were formed on R5A-I, N50A, R1N50A, and R2N50A, respectively. The amount of carbon in N50A was about two times higher than that of the other catalysts containing Rh metal. Rh metal promoted the gasification or reforming of adsorbed carbon species on Rh-Ni-Al-based catalysts during steam

reforming of sulfur-doped n-hexadecane [33]. Therefore, this metal was helpful in resisting deposition of carbon from the C_2H_4 product onto the catalytic surface.
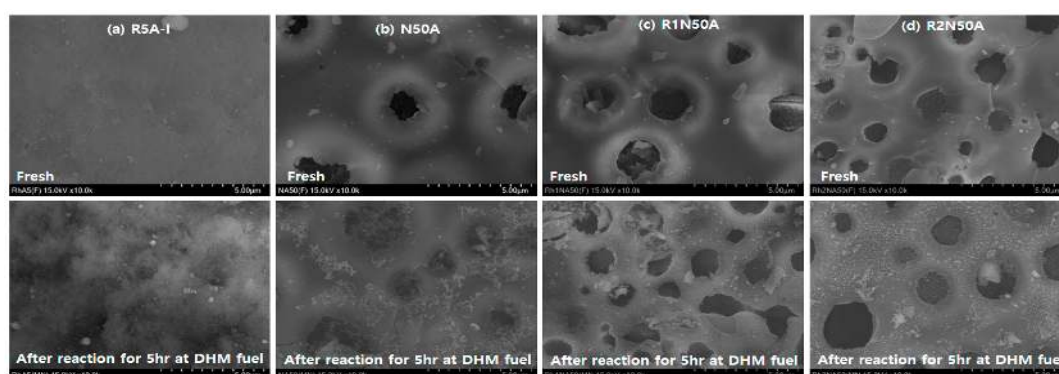

Figure 7. Scanning electron micrographs of (**a**) R5A-I, (**b**) N50A, (**c**) R1N50A, and (**d**) R2N50A.

Table 4. Amount of carbon on the catalytic surface of R5A-I, N50A, R1N50A, and R2N50A after 5-hour reactions of DHM fuel.

	R5A-I	**N50A**	**R1N50A**	**R2N50A**
Carbon (wt.%)	20.89	40.59	22.05	21.21

3. Materials and Methods

3.1. Catalyst Preparation

In our previous studies, various Ni-Al-based catalysts with Fe and Rh promoters were prepared by means of a polymer modified incipient method, to demonstrate the potential of this catalyst preparation method for hydrocarbon fuel reforming [41,42]. The following nomenclature was used for the catalysts: The letters 'N', 'R', 'F', and 'A' represent Ni, Rh, Fe, and Al metal, respectively. In addition, the figures revealed the content (wt.%) of metal oxide. During the catalyst preparation procedure, known amounts of $Ni(NO_3)_2 \cdot 6H_2O$ and $Al(NO_3)_3 \cdot 9H_2O$ were dissolved in ethylene glycol (15 mL) and methyl alcohol (15 mL). $Fe(NO_3)_3 \cdot 9H_2O$ and $Rh(NO_3)_3 \cdot xH_2O$ were added as the precursors for Fe and Rh metal. The solid products were obtained by heating the solutions with PMMA colloidal crystals (1.5 g) on a hot plate at 100 °C and drying at 300 °C for 4 hours. Afterward, the products were calcined at 800 °C for 4 hours. An Rh-Al-based catalyst (R5A-I) was prepared using a conventional impregnation method, and the catalytic performance of this catalyst was compared with that of the other catalysts. $Rh(NO_3)_3 \cdot xH_2O$ and γ-Al_2O_3 were dissolved in water. The resulting solution was stirred at room temperature and the suspension was then evaporated via vacuum evaporation. Afterward, the powder was dried at 300 °C for 4 hours and then calcined at 800 °C for 4 hours as per the above conditions.

3.2. Catalytic Reforming Tests

The catalysts (mass: 0.5 g, size: 150 to 250 μm) were supported by quartz wool on either side and packed in the middle of a fixed-bed quartz reactor. The quartz reactor was generally used to minimize coke formation on the inner walls. Thermocouple was placed at the center of the catalytic bed and controlled the temperature of the electric furnace. In addition, the temperature was monitored in the inlet and outlet of the reactor. The temperature gradient between the inlet and outlet of the reactor and the catalytic bed was negligible. The mass flow controllers were used to adjust the flow rate of gases such as H_2, N_2, and O_2. Enough gas was introduced and the line was heated to prevent condensation. The diesel surrogate fuel was prepared from dodecane ($C_{12}H_{26}$), hexadecane ($C_{16}H_{34}$), and 1-methylnaphthalene ($C_{11}H_{10}$). This fuel varied depending on whether aromatic hydrocarbons (e.g., $C_{11}H_{10}$) were contained in diesel surrogate fuels such as DH ($C_{12}H_{26}$ and $C_{16}H_{34}$ mixture)

and DHM (DH fuel and $C_{11}H_{10}$ mixture) fuel. The selected diesel surrogate fuel and H_2O were injected by syringe pumps and completely vaporized with N_2 at 400 °C in the vaporizer. Afterward, the condensable liquids were completely removed before injection into gas chromatograph (GC, Agilent 6890, Santa Clara, CA, USA). Product gases such as H_2, N_2, CO, CH_4, and CO_2 were then analyzed via GC-TCD (thermal conductivity detector). Supplementary Materials Figure S2 shows the schematic diagram of experimental apparatus. In addition, CO_2 and hydrocarbons, such as ethane (C_2H_6), ethylene (C_2H_4), propylene (C_3H_6), 1,3-butadiene (C_4H_6), 1,3-cyclopentadiene (C_5H_6), benzene (C_6H_6), and toluene (C_7H_8), were detected via GC-MS (Agilent (7890B-5977B GC/MSD), Santa Clara, CA, USA). The H_2 pre-reduction treatments were conducted for 2 hours at 750 °C prior to the tests. The catalytic performance of each catalyst was investigated under the following conditions: S/C = 1.17, O_2/C = 0.24, 750 °C, and GHSV = 12,000 h^{-1} at DH or DHM fuel. The diesel surrogate fuel conversions and the selectivity of product gases were calculated as follows.

$$\text{Conversion (\%)} = \left(\frac{F_{CO \cdot Out} + F_{CO_2 \cdot Out} + F_{CH_4 \cdot Out}}{F_{C_{12}H_{26} \cdot In} \times 12 + F_{C_{16}H_{34} \cdot In} \times 16 + F_{C_{11}H_{10} \cdot In} \times 11} \right) \times 100 \tag{1}$$

$$\text{Selectivity of product gas (\%)} = \left(\frac{F_{product \cdot Out}}{F_{H_2 \cdot Out} + F_{CO \cdot Out} + F_{CH_4 \cdot Out} + F_{CO_2 \cdot Out}} \right) \times 100 \tag{2}$$

3.3. Characterization

The morphology and the amounts of carbon on the catalytic surface were determined via FE-SEM (S-4300, Hitachi, Tokyo, Japan) and EDX (EDX-350, Hitachi, Tokyo, Japan), respectively. The crystal structure of each catalyst was determined via XRD using a CuKα radiation source (Phillips XPERT instrument, Korea Basic Science Institute, Daegu). Furthermore, the phases comprising the mixed metal oxides were identified via XPS (Quantera SXM, ULVAC-PHI, Chigasaki, Japan).

4. Conclusions

To investigate the effect of aromatic hydrocarbon on the autothermal reforming of diesel, 1-methylnaphthalene ($C_{11}H_{10}$) was selected and blended as an aromatic hydrocarbon. Two types of diesel surrogate fuel, i.e., DH ($C_{12}H_{26}$ and $C_{16}H_{34}$ mixture) and DHM (DH fuel and $C_{11}H_{10}$ mixture) fuels, were prepared. The R5A-I, Ni-Al-based catalyst, and Fe-Ni-Al-based catalyst maintained catalytic performances for 5 hours using DH fuel, whereas the catalysts except for R5A-I became deactivated at DHM fuel. Unsurprisingly, the Fe promoter of the Ni-Al-based catalysts yielded no improvement in the catalytic performance at DHM fuel. When an Rh metal was added to these catalysts, the resulting catalytic performance was superior to that achieved for the other catalysts. The extent of catalyst deactivation decreased with greater content of this metal as a promoter. Although expensive, the Rh metal acted as a remarkable promoter that improved the resistance property of aromatic carbon for autothermal reforming of diesel fuel. The GC-MS data revealed that, among the produced hydrocarbons, C_2H_4 played a major role in deactivating the catalysts, since this hydrocarbon resulted in carbon deposition that covered the Ni metal active sites. In conclusion, the catalytic performance of Ni-Al-based catalysts, which are susceptible to accelerated carbon deposition from the C_2H_4 product, can be improved through the addition of small amounts of Rh metal.

Supplementary Materials: The following are available online at http://www.mdpi.com/2073-4344/9/7/573/s1. Figure S1: Conversions of the blank test, N10A, N30A, and N50A at DHM fuel, Figure S2 The schematic diagram of experimental apparatus.

Author Contributions: Conceptualization, D.G.J., D.S.H., and S.Y.J. Data curation, T.Y.K. and H.J.C. Investigation, D.G.J. and D.S.H. Supervision, S.Y.J., S.C.L., and J.C.K. Writing – original draft, D.C.J. Writing – review & editing, S.B.J.

Conflicts of Interest: The authors declare no conflict of interest.

References

1. Balat, M. Potential importance of hydrogen as a future solution to environmental and transportation problems. *Int. J. Hydrogen Energy* **2008**, *33*, 4013–4029. [CrossRef]

2. Afgan, N.; Veziroglu, A. Sustainable resilience of hydrogen energy system. *Int. J. Hydrogen Energy* **2012**, *37*, 5461–5467. [CrossRef]

3. Zheng, J.; Liu, X.; Xu, P.; Liu, P.; Zhao, Y.; Yang, J. Development of high pressure gaseous hydrogen storage technologies. *Int. J. Hydrogen Energy* **2012**, *37*, 1048–1057. [CrossRef]

4. Megede, D.Z. Fuel processors for fuel cell vehicles. *J. Power Sources* **2002**, *106*, 35–41. [CrossRef]

5. Aicher, T.; Lenz, B.; Gschnell, F.; Groos, U.; Federici, F.; Caprile, L.; Parodi, L. Fuel processors for fuel cell APU applications. *J. Power Sources* **2006**, *154*, 503–508. [CrossRef]

6. Lindström, B.; Karlsson, J.A.J.; Ekdunge, P.; De Verdier, L.; Häggendal, B.; Dawody, J.; Nilsson, M.; Pettersson, L.J. Diesel fuel reformer for automotive fuel cell applications. *Int. J. Hydrogen Energy* **2009**, *34*, 3367–3381. [CrossRef]

7. Yoon, S.H.; Bae, J.M.; Lee, S.H.; Pham, T.V.; Katikaneni, S.P. A diesel fuel processor for stable operation of solid oxide fuel cells system: II. Integrated diesel fuel processor for the operation of solid oxide fuel cells. *Int. J. Hydrogen Energy* **2012**, *37*, 9228–9236. [CrossRef]

8. Yoon, S.H.; Bae, J.M. A diesel fuel processor for stable operation of solid oxide fuel cells system: I. Introduction to post-reforming for the diesel fuel processor. *Catal. Today* **2010**, *156*, 49–57. [CrossRef]

9. Gerardo, V.H.; Johanan, Á.J.; Tobias, M.; Michael, D.; Keno, L.; Stephan, K. Exergy analysis of the diesel pre-reforming SOFC-system with anode off-gas recycling in the SchIBZ project. Part II: System exergetic evaluation. *Int. J. Hydrogen Energy* **2019**, *44*, 10916–10924.

10. Bali, A.; Blanchard, J.; Chamoumi, M.; Abatzoglou, N. Bio-Oil Steam Reforming over a Mining Residue Functionalized with Ni as Catalyst Ni-UGSO. *Catalysts* **2018**, *8*, 1. [CrossRef]

11. Kim, D.H.; Kang, J.S.; Lee, Y.J.; Park, N.K.; Kim, Y.C.; Hong, S.I.; Moon, D.J. Steam reforming of n-hexadecane over noble metal-modified Ni-based catalysts. *Catal. Today* **2008**, *136*, 228–234. [CrossRef]

12. Fauteux-Lefebvre, C.; Abatzoglou, N.; Blanchard, J.; Gitzhofer, F. Steam reforming of liquid hydrocarbons over a nickel-alumina spinel catalyst. *J. Power Sources* **2010**, *195*, 3275–3283. [CrossRef]

13. Peymani, M.; Alavi, S.M.; Arandiyan, H.; Rezaei, M. Rational Design of High Surface Area Mesoporous Ni/CeO$_2$ for Partial Oxidation of Propane. *Catalysts* **2018**, *8*, 388. [CrossRef]

14. Navarro, R.M.; Alvarez-Galvan, M.C.; Rosa, F.; Fierro, J.L.G. Hydrogen production by oxidative reforming of hexadecane over Ni and Pt catalysts supported on Ce/La-doped Al$_2$O$_3$. *Appl. Catal. A Gen* **2006**, *297*, 60–72. [CrossRef]

15. Wang, Z.; Huang, H.; Liu, H.; Zhou, X. Self-sustained electrochemical promotion catalysts for partial oxidation reforming of heavy hydrocarbons. *Int. J. Hydrogen Energy* **2012**, *37*, 17928–17935. [CrossRef]

16. Kang, I.Y.; Bae, J.M. Autothermal reforming study of diesel for fuel cell application. *J. Power Sources* **2006**, *159*, 1283–1290. [CrossRef]

17. Deivanayagam, H.; Ruinan, Y.; Yingcong, Z.; Brian, G.; Sotirios, M.; Robyn, E.S.; Michael, A.L.; Marco, J.C.; Rajinder, G.; Andrew, D.; et al. Catalytic partial oxidation reformation of diesel, gasoline, and natural gas for use in low temperature combustion engines. *Fuel* **2019**, *246*, 295–307.

18. Savvas, L.D.; Nikolaos, D.C.; Kyriakos, N.P.; Maria, A.G. Green Diesel: Biomass Feedstocks, Production Technologies, Catalytic Research, Fuel Properties and Performance in Compression Ignition Internal Combustion Engines. *Energies* **2019**, *12*, 809.

19. Parmar, R.D.; Kundu, A.; Karan, K. Thermodynamic analysis of diesel reforming process: Mapping of carbon formation boundary and representative independent reactions. *J. Power Sources* **2009**, *194*, 1007–1020. [CrossRef]

20. Mueller, C.J.; Cannella, W.J.; Bays, J.T.; Bruno, T.J.; DeFabio, K.; Dettman, H.D.; Gieleciak, R.M.; Huber, M.L.; Kweon, C.B.; McConnell, S.S.; et al. Diesel Surrogate Fuels for Engine Testing and Chemical-Kinetic Modeling: Compositions and Properties. *Energy Fuels* **2016**, *30*, 1445–1461.

21. Gonzalez, A.V.; Pettersson, L.J. Full-scale autothermal reforming for transport applications: The effect of diesel fuel quality. *Catal. Today* **2013**, *210*, 9–25. [CrossRef]

22. Huseyin, A. Effect of impregnation sequence of Mg on performance of mesoporous alumina supported Ni catalyst in dry reforming of methane. *Int. J. Hydrogen Energy* **2018**, *43*, 6561–6574.

23. Dori, Y.K.; Kristian, S.; Yiying, J.; Wakshum, M.T.; Zhixin, Y. Biogas dry reforming for syngas production on La promoted hydrotalcite-derived Ni catalysts. *Int. J. Hydrogen Energy* **2018**, *43*, 19438–19450.

24. Norazimah, H.; Sumaiya, Z.A.; Osarieme, U.O.; Yun, H.T.; Mohammad, T.A. Hydrogen production from glycerol dry reforming over Ag-promoted Ni/Al_2O_3. *Int. J. Hydrogen Energy* **2019**, *44*, 213–225.

25. Zhanfeng, H.; Yi, J.; Jianli, W.; Yaoqiang, C. Bi-functional composite oxides M(Na, K)-Ni/La-Al_2O_3 catalysts for steam reforming of n-decane. *Fuel* **2018**, *212*, 193–201.

26. Ferrandon, M.; Krause, T. Role of the oxide support on the performance of Rh catalysts for the autothermal reforming of gasoline and gasoline surrogates to hydrogen. *Appl. Catal. A Gen* **2006**, *311*, 135–145. [CrossRef]

27. Tribalis, A.; Panagiotou, G.D.; Bourikas, K.; Sygellou, L.; Kennou, S.; Ladas, S.; Lycourghiotis, A.; Kordulis, C. Ni Catalysts Supported on Modified Alumina for Diesel Steam Reforming. *Catalysts* **2016**, *6*, 11. [CrossRef]

28. Hanyu, C.; Xi, W.; Zhixiang, P.; Hongming, X. Numerical Simulation and Experimental Investigation of Diesel Fuel Reforming over a Pt/CeO_2-Al_2O_3 Catalyst. *Energies* **2019**, *12*, 1056.

29. Cai, W.J.; Qian, L.P.; Yue, B.; He, H.Y. Rh doping effect on coking resistance of Ni/SBA-15 catalysts in dry reforming of methane. *Chin. Chem. Lett.* **2014**, *25*, 1411–1415. [CrossRef]

30. Hou, Z.; Yashima, T. Small amounts of Rh-promoted Ni catalysts for methane reforming with CO_2. *Chin. Chem. Lett.* **2003**, *89*, 3–4.

31. Strohm, J.J.; Zheng, J.; Song, C. Low-temperature steam reforming of jet fuel in the absence and presence of sulfur over Rh and Rh-Ni catalysts for fuel cells. *J. Catal.* **2006**, *238*, 309–320. [CrossRef]

32. Kaila, R.K.; Gutierrez, A.; Krause, A.O.I. Autothermal reforming of simulated and commercial diesel: The performance of zirconia-supported RhPt catalyst in the presence of sulfur. *Appl. Catal. B Environ.* **2008**, *84*, 324–331. [CrossRef]

33. Lakhapatri, S.L.; Abraham, M.A. Deactivation due to sulfur poisoning and carbon deposition on Rh-Ni/Al_2O_3 catalyst during steam reforming of sulfur-doped n-hexadecane. *Appl. Catal. A Gen.* **2009**, *364*, 113–121. [CrossRef]

34. Karatzas, X.; Jansson, K.; Gonzalez, A.; Dawody, J.; Pettersson, L.J. Autothermal reforming of low-sulfur diesel over bimetallic RhPt supported on Al_2O_3, CeO_2-ZrO_2, SiO_2 and TiO_2. *Appl. Catal. B Environ.* **2011**, *106*, 476–487. [CrossRef]

35. Zheng, Q.; Janke, C.; Farrauto, R. Steam reforming of sulfur-containing dodecane on a Rh-Pt catalyst: Influence of process parameters on catalyst stability and coke structure. *Appl. Catal. B Environ.* **2014**, *160–161*, 525–533. [CrossRef]

36. Vita, A.; Italiano, C.; Pino, L.; Lagana, M.; Recupero, V. Hydrogen-rich gas production by steam reforming of n-dodecane. Part II: Stability, regenerability and sulfur poisoning of low loading Rh-based catalyst. *Appl. Catal. B Environ.* **2017**, *218*, 317–326. [CrossRef]

37. Karatzas, X.; Dawody, J.; Grant, A.; Svensson, E.E.; Pettersson, L.J. Zone-coated Rh-based monolithic catalyst for autothermal reforming of diesel. *Appl. Catal. B Environ.* **2011**, *101*, 226–238. [CrossRef]

38. Karatzas, X.; Jansson, K.; Dawody, J.; Lanza, R.; Pettersson, L.J. Microemulsion and incipient wetness prepared Rh-based catalyst for diesel reforming. *Catal. Today* **2011**, *175*, 515–523. [CrossRef]

39. Shoynkhorova, T.B.; Simonov, P.A.; Potemkin, D.I.; Snytnikov, P.V.; Belyaev, V.D.; Ishchenko, A.V.; Svintsitskiy, D.A.; Sobyanin, V.A. Highly dispersed Rh-, Pt-, Ru/$Ce_{0.75}Zr_{0.25}O_2$−δ catalysts prepared by sorption-hydrolytic deposition for diesel fuel reforming to syngas. *Fuel* **2018**, *237*, 237–244.

40. Rogozhnikov, V.N.; Kuzin, N.A.; Snytnikov, P.V.; Potemkin, D.I.; Shoynkhorova, T.B.; Simonov, P.A.; Shilov, V.A.; Ruban, N.V.; Kulikov, A.V.; Sobyanin, V.A. Design, scale-up, and operation of a Rh/$Ce_{0.75}Zr_{0.25}O_{2-δ}$-η-$Al_2O_3$/FeCrAl alloy wire mesh honeycomb catalytic module in diesel autothermal reforming. *Chem. Eng. J.* **2019**, *374*, 511–519. [CrossRef]

41. Lee, W.S.; Ju, D.G.; Jung, S.Y.; Lee, S.C.; Ha, D.S.; Hwang, B.W.; Kim, J.C. N-Dodecane Autothermal Reforming Properties of Ni-Al Based Catalysts Prepared by Various Methods. *Top. Catal* **2017**, *60*, 727–734. [CrossRef]

42. Jung, S.Y.; Ju, D.G.; Lim, E.J.; Lee, S.C.; Hwang, B.W.; Kim, J.C. Study of sulfur-resistant Ni–Al-based catalysts for autothermal reforming of dodecane. *Int. J. Hydrogen Energy* **2015**, *40*, 13412–13422. [CrossRef]

43. Yoon, S.H.; Kang, I.Y.; Bae, J.M. Effects of ethylene on carbon formation in diesel autothermal reforming. *Int. J. Hydrogen Energy* **2008**, *33*, 4780–4788. [CrossRef]

44. Trabold, T.A.; Lylak, J.S.; Walluk, M.R.; Lin, J.F.; Troiani, D.R. Measurement and analysis of carbon formation during diesel reforming for solid oxide fuel cells. *Int. J. Hydrogen Energy* **2012**, *37*, 5190–5201. [CrossRef]

45. Jo, S.B.; Ju, D.G.; Jung, S.Y.; Ha, D.S.; Chae, H.J.; Lee, S.C.; Kim, J.C. Performance of an Auto-Reduced Nickel Catalyst for Auto-Thermal Reforming of Dodecane. *Catalysts* **2018**, *8*, 371. [CrossRef]

46. Bang, Y.; Han, S.J.; Seo, J.G.; Youn, M.H.; Song, J.H.; Song, I.K. Hydrogen production by steam reforming of liquefied natural gas (LNG) over ordered mesoporous nickel–alumina catalyst. *Int. J. Hydrogen Energy* **2012**, *37*, 17967–17977. [CrossRef]

47. Seo, J.G.; Youn, M.H.; Bang, Y.J.; Song, I.K. Effect of NiAl atomic ratio of mesoporous Ni-Al$_2$O$_3$ aerogel catalysts on their catalytic activity for hydrogen production by steam reforming of liquefied natural gas (LNG). *Int. J. Hydrogen Energy* **2010**, *35*, 12174–12181. [CrossRef]

48. Wang, Y.; Song, Z.; Ma, D.; Luo, H.; Liang, D.; Bao, X. Characterization of Rh-based catalysts with EPR, TPR, IR and XPS. *J. Mol. Catal. A: Chem* **1999**, *149*, 51–61. [CrossRef]

49. Osaki, T.; Mori, T. Characterization of nickel-alumina aerogels with high thermal stability. *J. Non-Cryst. Solids* **2009**, *355*, 1590–1596. [CrossRef]

50. Obu-Cann, K.; Tokutaka, H.; Fujimura, K.; Yoshihara, K.; Metal Materials Group of SASJ. Chemical Analysis of XPS (X-ray Photoelectron Spectroscopy) Data using Self-Organising Maps. *J. Surf. Anal.* **1999**, *6*, 85–86.